Study of $Li^6 + C^{12}$ Reactions*

D. J. Johnson† and M. A. Waggoner
Department of Physics and Astronomy, The University of Iowa, Iowa City, Iowa 52240
(Received 22 October 1969)

A comprehensive investigation of the $Li^6 + C^{12}$ reaction has been carried out for particle groups corresponding to the following states of the residual nuclei involved: 0.0, 0.871, 3.058, 3.846, and 4.551 MeV for O^{17}; 0.0, 6.05+6.13 (unresolved), 6.92+7.12, and 8.88 MeV for O^{16}; 0.0 MeV for O^{15}; and 0.0, 3.945, and 4.91+5.10 MeV for N^{14}. Yield curves were measured for protons, deuterons, and α particles at laboratory angles of 0° and 40°, at Li^6 bombarding energies from 5.6 to 14.0 MeV. Angular distributions were measured at 9.0, 10.0, 11.2, 12.0, 13.0, and 14.0 MeV for all of the above groups and from 5.6 to 6.6 MeV at 0.200-MeV intervals for most of the groups.

A comparison has been made of the accumulated α-particle data and two-mode plane-wave and single-mode distorted-wave direct-reaction models. The proton, deuteron, and α-particle data were also compared with the statistical compound-nucleus model.

I. INTRODUCTION

In the present experiment all resolvable reaction products from the $C^{12}(Li^6, p)O^{17}$, $C^{12}(Li^6, d)O^{16}$, $C^{12}(Li^6, t)O^{17}$, and $C^{12}(Li^6, d)N^{14}$ reactions were studied at Li^6 bombarding energies of 5.6 to 6.6 and 9.0 to 14.0 MeV. The Q values of the various reactions[1] are given in Fig. 1. Spins and parities of the levels are taken from Ref. 1, except for the spin of the 3.846-MeV level[2] of O^{17}. The experimental data obtained and presented for these reactions consist of angular distributions at bombarding energies from 5.6 to 6.6 MeV at 200-keV intervals and at 9.0, 10.0, 11.2, 12.0, 13.0, and 14.0 MeV, and of yield curves at $\theta_{lab} = 0°$ and 40°. In addition, an angular distribution of Li^6 elastically scattered from C^{12} was obtained at a bombarding energy of 13.0 MeV for use in determining optical-model parameters for the $Li^6 + C^{12}$ entrance channel.

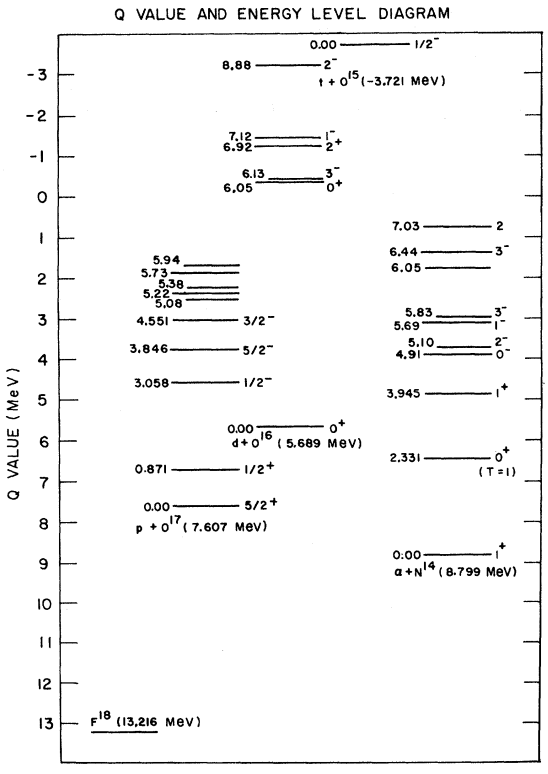

FIG. 1. Q-value and energy-level diagram.

A comparison has been made of the results of the experiment and predictions of direct-reaction and statistical compound-nucleus models.

II. EXPERIMENTAL

This experiment was performed with a Li^6 beam from the University of Iowa HVEC Model CN Van de Graaff accelerator. Lithium beam energies in excess of 6.6 MeV were obtained using carbon stripping foils in the accelerator tube. The beam energy has been shown to be stable and accurate to ±0.3% over long periods of operation.

The target chamber used for this experiment was a 17-in.-diam ORTEC Model 600 scattering chamber. A detector-foil-changer assembly which contained a ΔE, E detector system was mounted on the top plate 14 cm from the target located at the center of the chamber. A monitor detector was mounted in the reaction plane on the chamber wall at 20° with respect to the beam. The beam was collimated to a spot 2 mm in diam with two collimator pairs located in the beam tube near the entrance to the chamber.

The ΔE and E detectors were solid-state detectors, the former 40 μ thick and the latter 2000 or 3000 μ thick, depending upon the energy range being studied. The aperature for this detector assembly subtended a solid angle of 1.49×10^{-3} sr

with respect to the center of the chamber.

The monitor detector was a solid-state detector with an aperture of 2.03×10^{-3} sr with respect to the target center, and was just thick enough to stop all incident α particles. Some segments of the 5.6- to 6.6-MeV data were taken at an early stage[3] of this experiment on apparatus described by Heikkinen.[4]

Pulses were amplified and routed via Canberra solid-state electronics to Nuclear Data analog-to-digital converters. The ADC's were coupled through an interface to an on-line Control Data 160A computer. Data corresponding to the detection of protons, deuterons, and tritons were stored in a 60- by 256-channel E, ΔE matrix. Since α particles produce a higher ΔE pulse than charge-one particles, they could be readily separated from charge-one events, and were stored in a single-parameter energy distribution. A single-parameter pulse-height distribution of the monitor events was stored in the computer simultaneously with the aquisition of the E, ΔE data. All of the data were transfered at the completion of each run onto magnetic tape.

Targets consisted of self-supporting foils obtained by evaporating carbon from an arc onto Teepol-coated slides. The targets, which were oriented at 45° during angular-distribution measurements and at 0° during yield-curve measurements, were selected to give an energy spread of the Li^6 beam in the target of no greater than 90 keV. Target thickness was measured to ±8% by determining the energy loss of α particles from a thorium C′ source in the target, and using stopping-power data of Williamson, Boujot, and Picard.[5] The targets ranged from 10 to 52 $\mu g/cm^2$ in thickness.

III. SOURCE OF ERROR

The yield curves measured at $\theta_{lab}=40°$ were used to normalize the angular distributions taken at different bombarding energies to absolute values. For the measurement of the 0° and 40° yield curves, the problem of carbon buildup was eliminated by surrounding the target with a capped aluminum cylinder, which served both as a hydrocarbon pump and a Faraday cup during yield-curve measurements. The relative error of the yield-curve points, excluding the statistical counting error is considered to be less than 7%.

Including possible error in the determination of target thickness and detector solid angle as well as that in absolute-current integration, the total absolute error of the 40° yield-curve data is considered to range from 10 to 15% (depending on the size of the statistical counting error of each yield-curve point). The absolute error of the 0° yield-curve points is judged to be about 20%, somewhat greater because the absolute values of these points were obtained by adjusting these data, via the angular-distribution data, to have the correct value relative to the 40° differential-cross-section values at energies for which angular distributions were measured.

The ground-state α-particle group was free of contaminants at $\theta_{lab}=20°$, and was used as a monitor group for normalization of the angular-distribution data at a given bombarding energy. The statistical counting error of this monitor group, combined with possible errors due to uncertainties in effective beam energy and detection angle, produce a random error of about 5% which must be combined with the statistical counting error of each angular-distribution point to give the relative errors for points on an angular distribution. The data taken earlier at 5.6 to 6.6 MeV with the older apparatus have been assigned a random error of 7.2% instead of the 5% of the later data. The error bars terminating in straight lines on the plots of the angular distributions are representative of statistical counting error only. Where statistical counting errors are smaller than the size of the points, the error bars are omitted. In cases where there were unusual problems due to background events, the error bars shown on the plots include possible error due to these events as well as statistical counting error, and are terminated by an arrow.

When the possible errors involved with the normalization of the angular distributions to the yield curves are accounted for, the absolute error of the angular-distribution data points ranges from 10 to 15% (depending upon the magnitude of the statistical counting error of the points), or up to about 20% in cases where background events were a problem.

IV. RESULTS

Experimental results for the particle groups which could be studied are presented in Figs. 2–19: typical energy spectra showing states excited by the reactions, in Figs. 2–4; the yield curves at laboratory angles of 0° and 40°, in Figs. 5 and 6; and the angular distributions, in Figs. 7–19. The different symbols used to plot the angular-distribution points represent data obtained from repeated runs during this experiment. Of the 5.6- to 6.6-MeV angular-distribution data, the dots represent data obtained with the older apparatus. The total cross sections are given in Table I, and compared to the $(2J+1)$ rule in Fig. 20.

A proton energy spectrum at a Li^6 bombarding

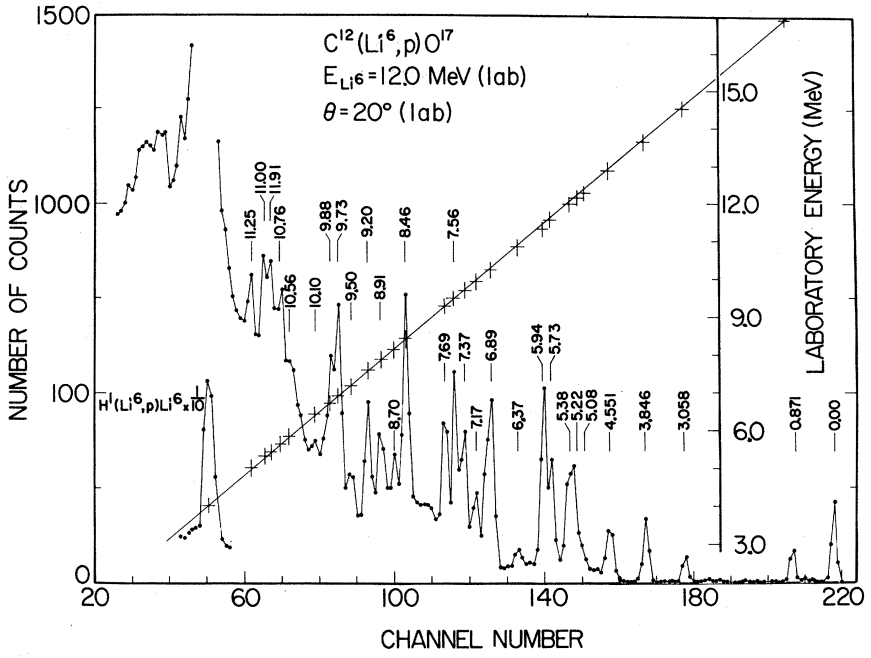

FIG. 2. Proton energy spectrum.

energy of 12.0 MeV is shown in Fig. 2. The energy levels in the residual nucleus associated with the observed peaks have been identified from kinematics, as were those in the other particle spectra. In particular, the diagonal line in this spectrum is the energy calibration curve used to determine the energy of the groups observed and identify the levels in O^{17} with which each is associated. The energy levels are those of Lauritsen and Ajzenberg-Selove.[1]

A proton continuum begins at a laboratory energy which corresponds to protons associated with the formation of O^{17} at an excitation of 4.15 MeV. This continuum is due to the three-body $O^{16}+p+n(+3.45$ MeV) final state. This continuum and the additional continuum from the $C^{13}+p+d(+1.25$ MeV) reaction limit the present investigation to the proton groups corresponding to the formation of the ground and first four excited states of O^{17}.

A typical deuteron spectrum is shown in Fig. 3. The continuum extending to an energy of 6.5 MeV in Fig. 3 is considered due to Coulomb breakup of Li^6 into a deuteron and α particle. This continuum limited the studies in this experiment to those deuteron groups associated with the formation of the 8.88-MeV or lower states in O^{16}. At angles greater than about 40°, the group corresponding to the 10.36-MeV state in O^{16} did not have sufficient energy to penetrate the ΔE detector and was therefore below the limit for particle identification by

TABLE I. Total cross sections (mb). The absolute error associated with all total cross sections is estimated to be ±15% unless otherwise noted.

E_{Li^6} (MeV)	P_0	P_1	P_2	P_3	P_4	d_0	d_1+d_4	d_3+d_4	d_5[a]	t_0[a]	α_0	α_2	$\alpha_3+\alpha_4$[a]
14.0	1.76	0.44	0.55	1.77	1.31	2.50	12.08	17.53	3.32	0.82	8.34	8.46	18.07
13.0	1.57	0.57	0.58	2.13	1.46	2.20	15.17	21.92	5.16	1.07	10.71	7.09	21.31
12.0	2.67	0.68	0.69	2.48	1.58	3.43	17.33	24.87	4.67	1.18	9.59	7.77	23.52
11.2	2.93	0.66	0.93	2.61	1.95	4.09	17.35	28.35	5.17	···	10.80	8.54	20.01
10.0	2.98	0.98	0.93	2.41	2.30	4.86	15.41	27.54	3.34	···	8.18	7.84	22.43
9.0	3.88	1.26	1.11	3.69	2.68	4.85	17.18	32.00	4.79	···	10.48	9.31	32.80
6.6	3.41	0.89	1.69	3.18	···	4.24	17.00	37.10	···	···	8.62	10.50	19.70
6.4	3.10	1.12	1.80	3.38	···	3.45	16.50	37.90	···	···	7.44	10.90	19.50
6.2	3.00	1.54	2.07	3.80	···	3.27	18.90	41.80	···	···	7.52	10.98	21.90
6.0	2.30	1.51	1.65	3.38	···	2.74	16.50	38.90	···	···	6.06	10.10	19.50
5.8	1.88	1.45	1.55	2.87	···	2.40	15.60	32.20	···	···	4.57	7.78	19.40
5.6	1.74	1.36	1.52	2.29	···	2.24	13.80	30.70	···	···	3.80	7.06	17.20

[a]The absolute error of the total cross sections associated with these groups is ±25%.

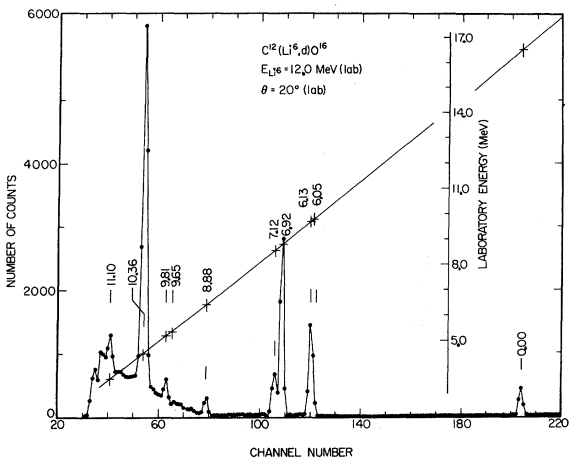

FIG. 3. Deuteron energy spectrum.

means of the E', ΔE system. No analysis was made on this group as a result. Similarly, the energy loss in the ΔE detector limited studies on the 8.88-MeV state to angles forward of 125° in the laboratory.

The doublet composed of the groups associated with the formation of the 6.05- and 6.13-MeV states in O^{16} was not resolved in this experiment. The second doublet group consisting of deuterons associated with the formation of the 6.92- and 7.12-MeV state in O^{16} is partially resolved at forward angles, but is almost completely unresolved at 90° because of $dE/d\theta$ across the detector. The doublet was analyzed as one group. In the region where it is resolved, the 6.92-MeV state has a yield about three times that of the 7.12-MeV state.

An α-particle spectrum is shown in Fig. 4. The α-particle groups associated with several states in the vicinity of the 9.0-MeV state in N^{14} were resolved, but the continuum from the $C^{13}+\alpha+p(+1.246$ MeV) three-body final state lies under these groups. This continuum and contaminant groups from the $Li^6+p \rightarrow He^3+\alpha(+4.02$ MeV) reaction, combined with the fact that at backward angles most of the groups associated with states above 5.10 MeV in N^{14} were too low in energy to be separated from charge-one particles, limited the α-particle groups for which useful angular-distribution measurements could be made to those associated with the ground, second, and third plus fourth excited states of N^{14}.

The predicted locations of α-particle groups from several low-lying states of N^{15} and F^{18} resulting from C^{13} and O^{16} contaminants are plotted in Fig. 4. The O^{16} and C^{13} contaminants produced α-particle groups which overshadowed the α-particle group corresponding to the 2.331-MeV isotopically forbidden first excited state of N^{14}, and allowed only an upper limit, 1% of the ground-state group, to be placed on its cross section.

The 5.6- to 6.6-MeV angular-distribution data are useful for comparison with the data at higher energies, and for noting the variation of the angular distributions with energy at these lower bombarding energies, but were not included in the sample used for comparison with theory.

At the higher energies, 9.0 to 14.0 MeV, angular distributions were taken at 1-MeV intervals except for the case of the distribution at 11.2 MeV. (The coherence width Γ_0 is of the order of 0.5

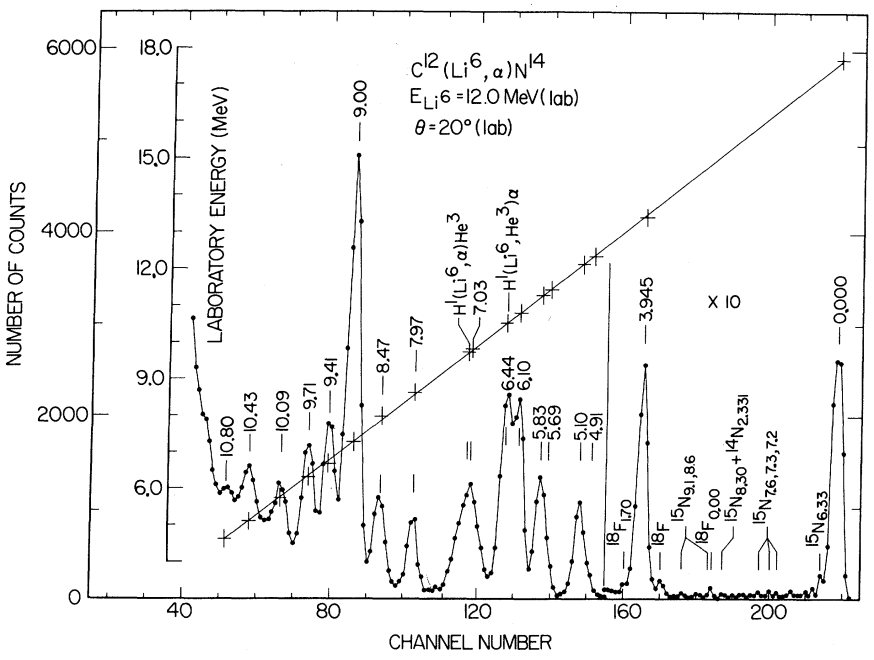

FIG. 4. α-particle energy spectrum. Weak groups resulting from O^{16} and C^{13} contaminants are denoted by the symbols for the residual nuclei involved.

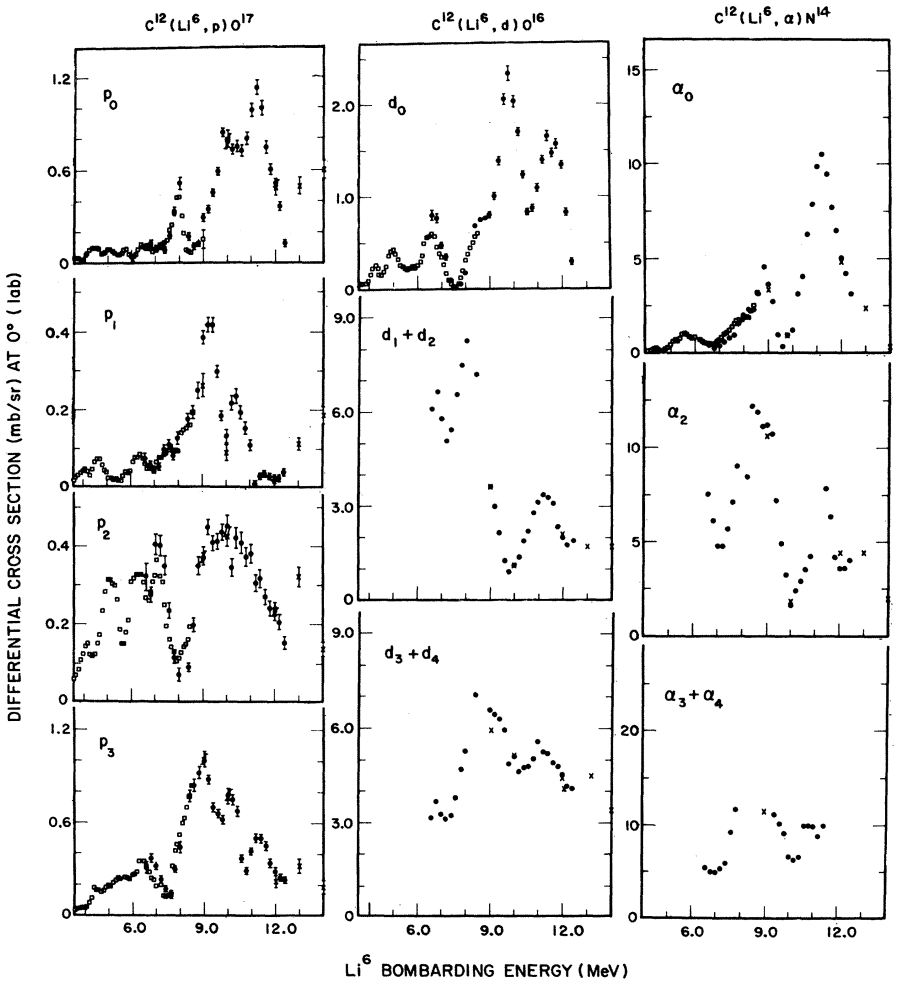

FIG. 5. Proton, deuteron, and α-particle yield curves measured at $\theta_{lab} = 0°$. The closed circles represent data accumulated during this experiment, and the crosses represent data taken from the angular-distribution measurements. The data plotted as squares have been reported by Dzubay[25] (all of Dzubay's data have been multiplied by 0.70). The data of Dzubay presented at 0° were taken at an effective angle of 6°.

MeV.) The planned 11.0-MeV distribution was taken at 11.2 MeV instead, because of the peak observed at this energy in both the 0° and 40° yield curves for several groups. No significant differences were observed in the angular distributions at this energy compared to these at adjacent energies, however.

The experimental values of the total cross sections are given in Table I. The total cross section for each group is seen to increase initially as a function of energy. Then, though the cross section for the α groups remains roughly constant with increasing energy, the cross section for other groups decreases quite rapidly with increasing energy.

V. COMPARISON OF RESULTS WITH VARIOUS MODELS

A. Direct-Reaction Model

An attempt was made to determine the importance of the direct-reaction mechanism for Li reactions studies here by fitting the α-particle angular distributions to a plane-wave two-mode model. For completeness, distorted-wave stripping calculations were also compared to the measured α-particle data.

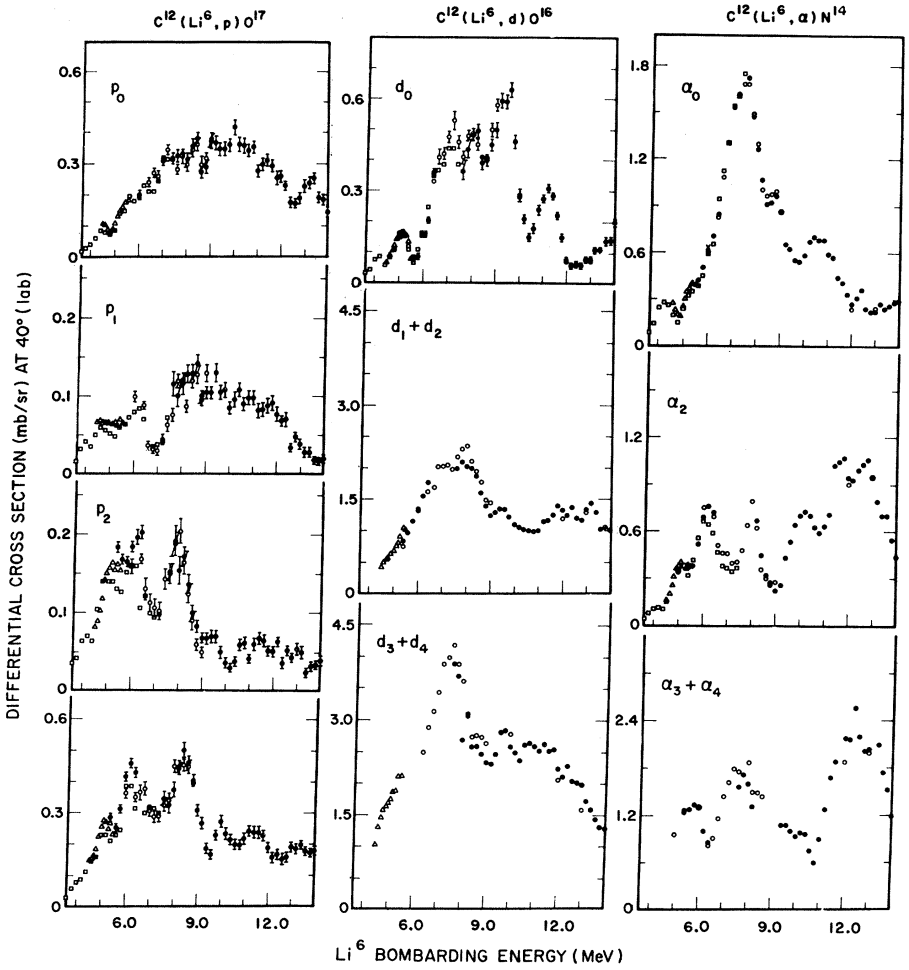

FIG. 6. Proton, deuteron, and α-particle yield curves measured at $\theta_{lab} = 40°$. The open and closed circles represent data accumulated at different times during this experiment. The triangles represent data reported by Heikkinen.[4] See caption of Fig. 5 for discussion of other symbols used for the data.

1. *Plane-Wave Born Approximation*

The basic form of the expression for the differential cross section used in the plane-wave two-mode case is that of Fulton and Owen[6] and Edwards.[7] The calculations were carried out for the pickup mode and exchange mode (heavy-particle stripping) for the inverse reaction $N^{14}(\alpha,Li^6)C^{12}$. Search programs used in two-mode calculations by one of the authors[8] were modified for use in this reaction. The differential cross section for the two-mode process can be expressed in terms of five parameters, four cutoff radii and the ratio of reduced widths for the two modes. The cutoff radii, corresponding to the lower limits of the Butler integrals for the pickup process and the corresponding radii for the exchange process, are associated with the following interacting systems:

pickup: r_1 for the d, α system,

a_1 for the C^{12}, d system;

exchange: r_2 for the α, Li^6 system,

a_2 for the Be^8, Li^6 system.

Calculations were initially made for the α_0 angular distributions assuming the N^{14} ground state to be a D state. This can be justified on the basis of the intermediate-coupling model[9] and from the β-decay probability[10] of C^{14}. It was possible to obtain reasonable fits considering only the D-state configuration, but the ratio of reduced widths (exchange/stripping) was found to be approximately 80. Since this ratio was many times too large, a 4% component of S state was included with the D component of the N^{14} ground state. When the search for a new set of parameters was made, only those

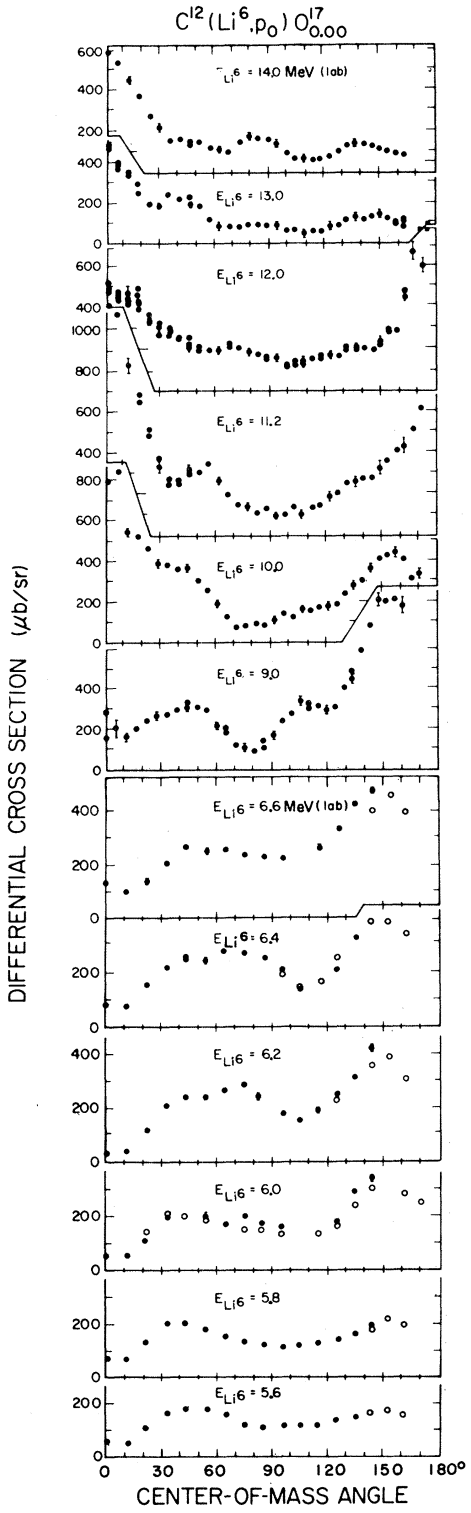

FIG. 7. Angular distributions for the p_0 group.

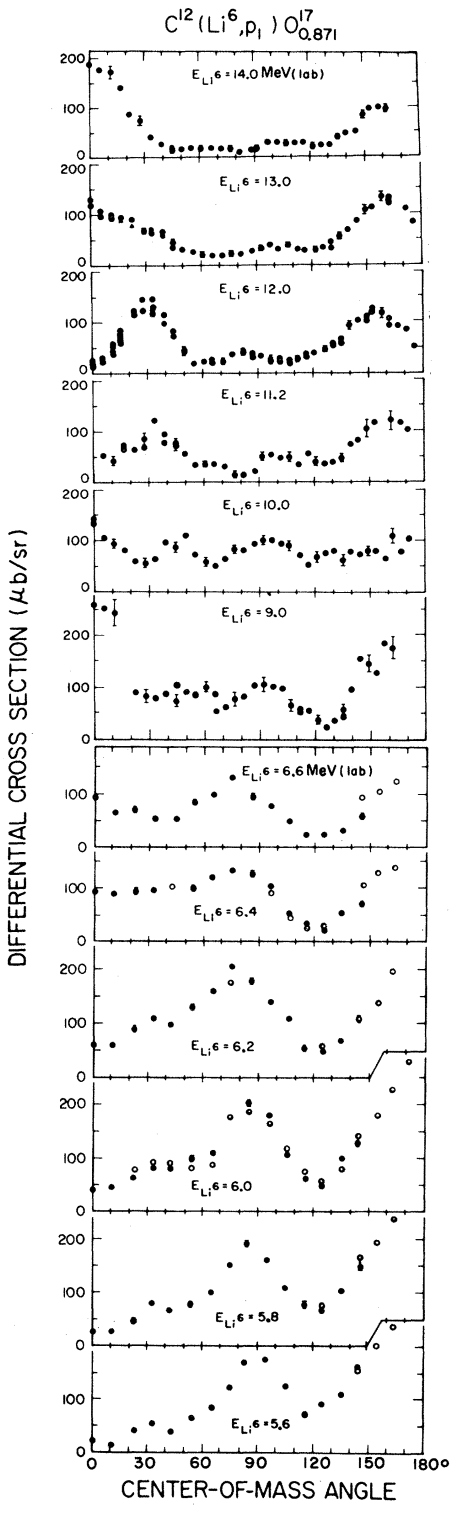

FIG. 8. Angular distributions for the p_1 group.

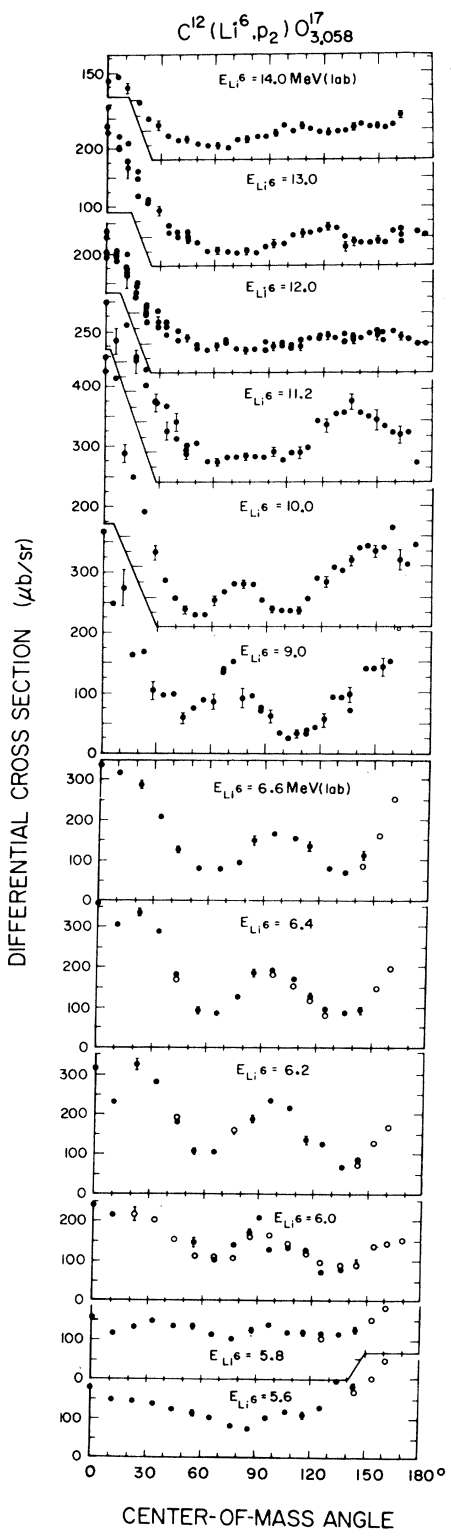

FIG. 9. Angular distributions for the p_2 group.

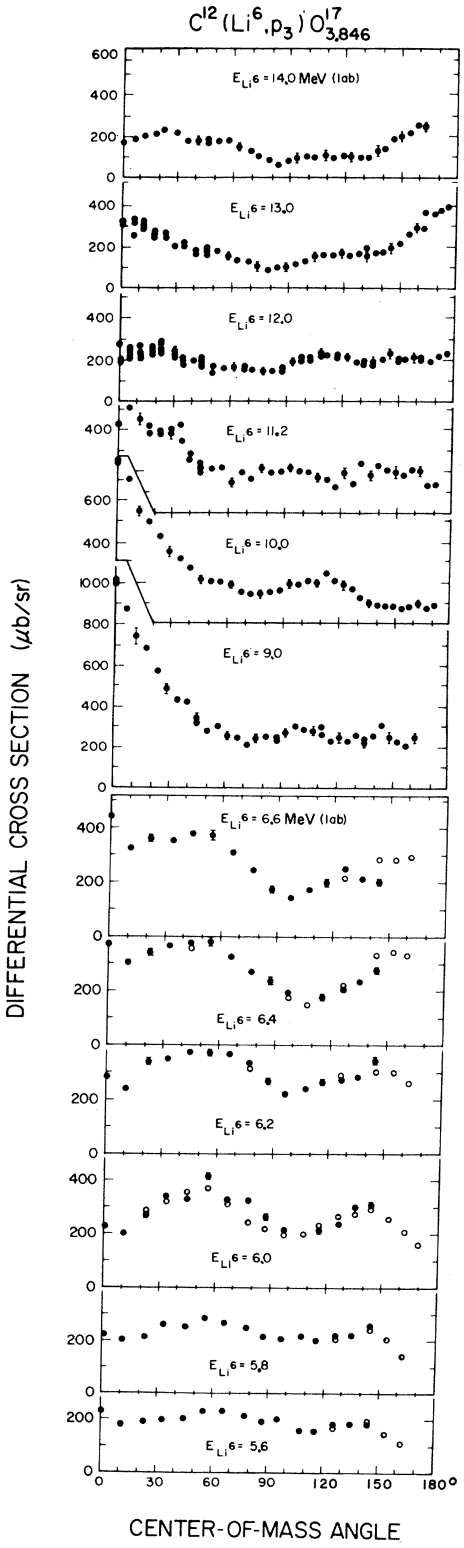

FIG. 10. Angular distributions for the p_3 group.

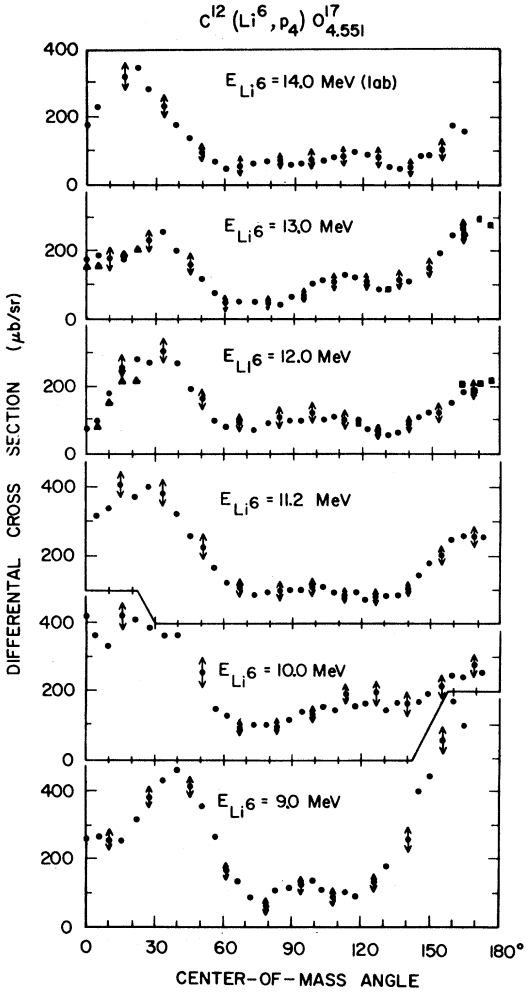

FIG. 11. Angular distributions for the p_4 group.

quantities related to N^{14} (namely a_1 and a_2) were allowed to be different for the S- and D-state configurations.

With the following radii, which were used at 14.0 MeV, the ratio of reduced widths for the two modes was determined to be 4.8 (assuming square wells for the interaction between the α, d and the Li^6, Be^8 systems):

S state: $r_1 = 2.70$ F, $a_1 = 2.75$ F,
$r_2 = 2.5$ F, $a_2 = 5.5$ F;
D state: $r_1 = 2.70$ F, $a_1 = 5.40$ F,
$r_2 = 2.5$ F, $a_2 = 6.5$ F.

It was also possible to obtain reasonable fits with those radii at Li^6 bombarding energies of 13.0, 12.0, and 11.2 MeV by setting r_1 equal to 3.1, 3.3 and 3.3 F, at the respective energies. The fits are shown in Fig. 21. For bombarding energies below

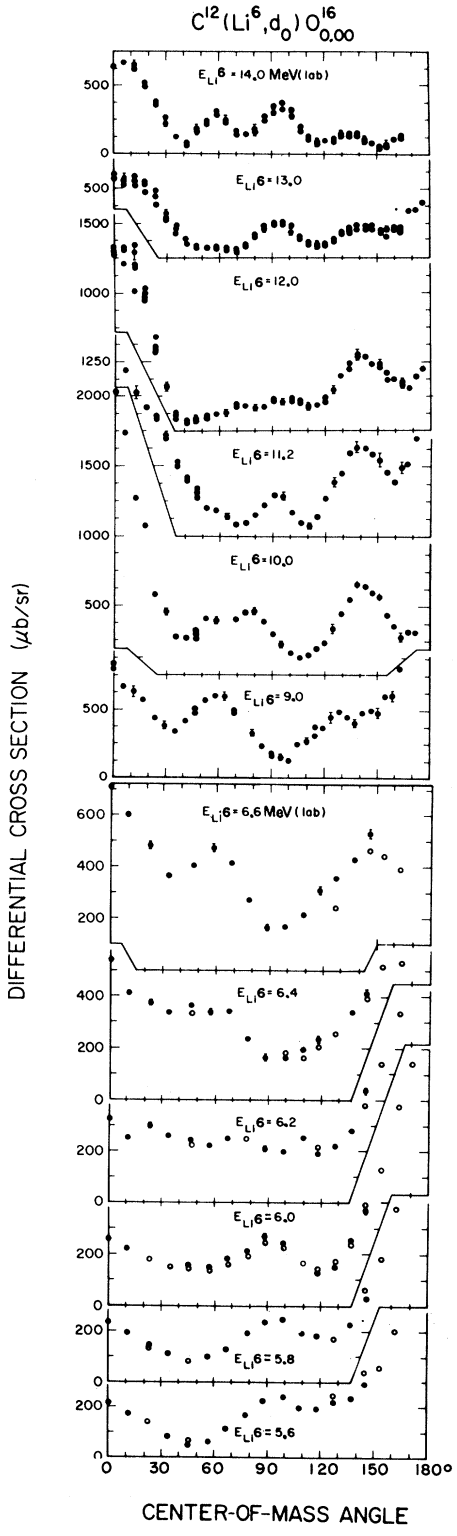

FIG. 12. Angular distributions for the d_0 group.

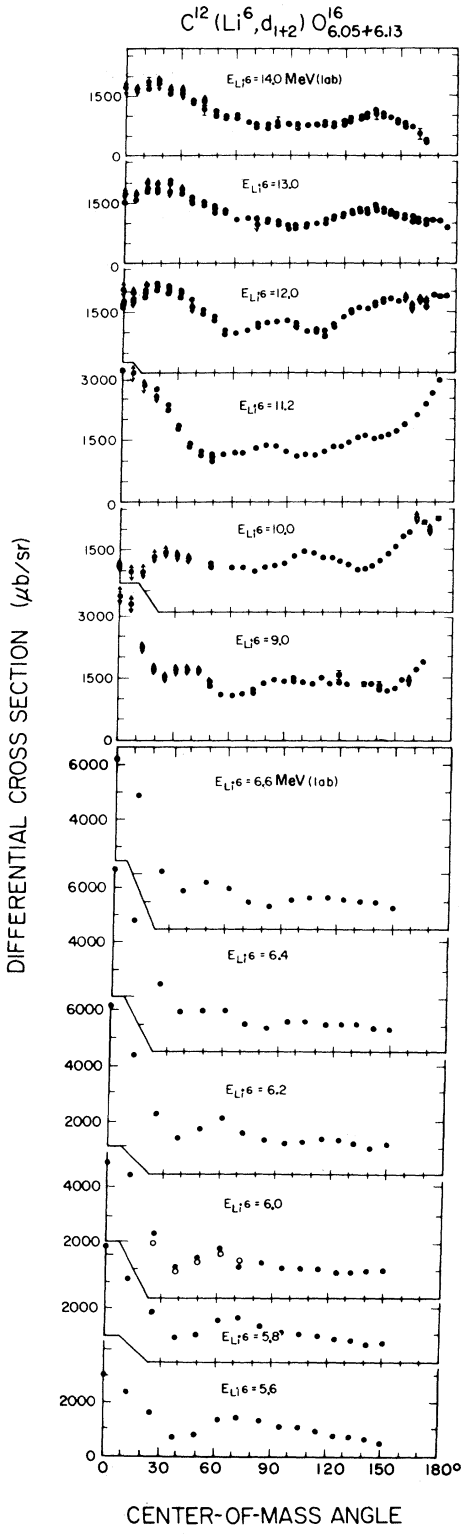

FIG. 13. Angular distributions for the d_1+d_2 groups.

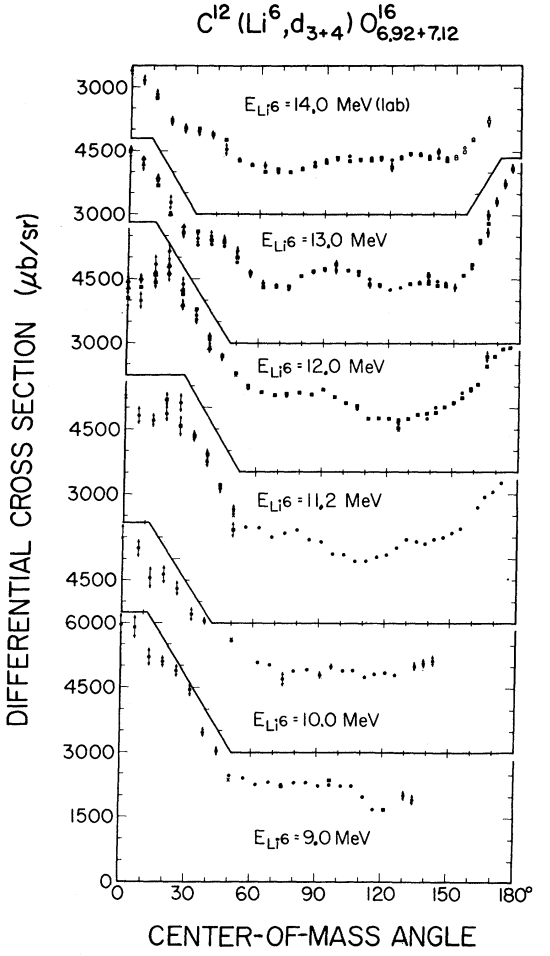

FIG. 14. Angular distributions for the d_3+d_4 groups.

11.2 MeV the fits become unreasonable with the above values of a_1, r_2, and a_2, but letting r_1 range from 2.7 to 3.3 F. The peaks in the backward-angle data were exactly out of phase with those in the theoretical calculations.

Some effort was spent attempting to find parameters which could reproduce the 9.0- and 10.0-MeV backward-angle data, but changes of the order of 10% for r_2 and 20% for $a_2(L=0)$ and $a_2(L=2)$ were not adequate.

The two-mode plane-wave calculations were not made for the second excited-state angular distribution for several reasons. Experience gained fitting the ground-state data indicates that it probably would not be possible to fit the 12.0-MeV data with the same parameters used at 13.0 and 14.0 MeV because of the shift in backward peaks at 12.0 MeV. The strong energy dependence of the 0° and 180° peaks is not consistent with the two-mode plane-wave model, since they can probably not be fit without varying parameters up and down to

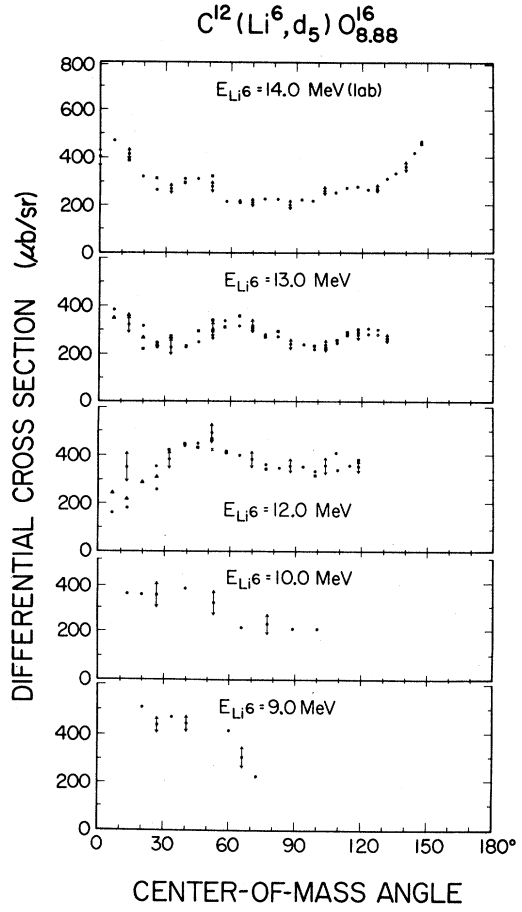

FIG. 15. Angular distributions for the d_5 group.

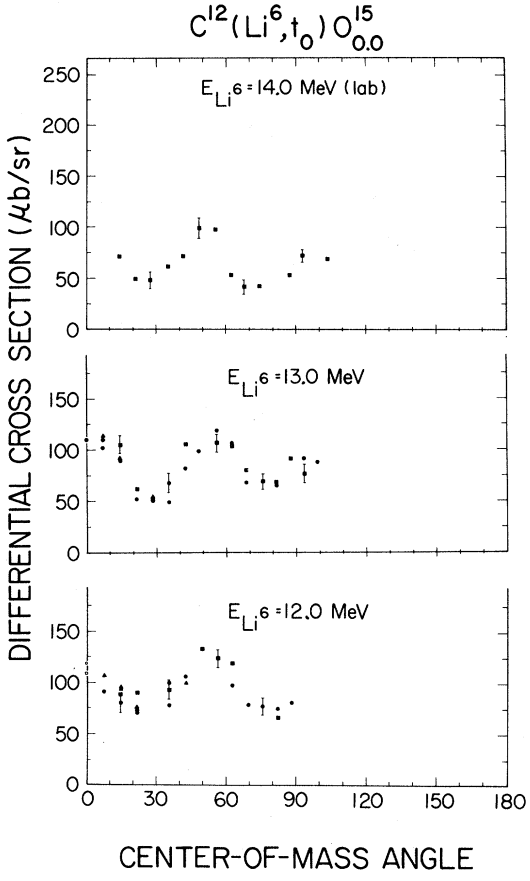

FIG. 16. Angular distributions for the t_0 group.

move peaks in and out of the nonphysical region to the left of 0° or to the right of 180°. And the anticipated computer costs and the time required to adequately determine the parameters was considered excessive for the information that might be obtained.

2. *Distorted-Wave Born Approximation*

Distorted-Wave Born-Approximation (DWBA) model calculations were made using computer code DRC.[11] This program assumes the interaction potential of the (α, d) system to be zero range and ignores target-recoil effects. The optical-model potential used has the form

$$U(r) = V_C(r) - V(1+e^{(r-R_1)/a})^{-1} - iWf(r),$$

where V_C is the Coulomb potential due to a uniformly charged sphere of radius R_1, and $f(r)$ is one of the following:

$$f_v = (1+e^{(r-R_2)/b})^{-1},$$
$$f_{sd} = -4bdf_v/dr,$$
$$f_G = e^{[-(r-R_2)/b]^2}.$$

The entrance-channel optical-model parameters were obtained from a parameter search of $Li^6 + C^{12}$ elastic scattering data (13.0 MeV) using an elastic scattering search routine written by Smith.[12] The fits for $C^{12}(Li^6, Li^6)C^{12}$ are shown in Fig. 22, and the parameters obtained are given in Table II. All DWBA calculations were made using parameter Set A for the entrance channel unless otherwise noted. The exit-channel parameters were obtained by a similar search on $N^{14}(\alpha, \alpha)N^{14}$ angular-distribution data (19.2 MeV) reported by Ploughe.[13]

Calculations for the α-particle angular distribution corresponding to the residual nucleus N^{14} in its ground state were made for 0 and 2 units of angular momentum transfer L and for cutoff radii R

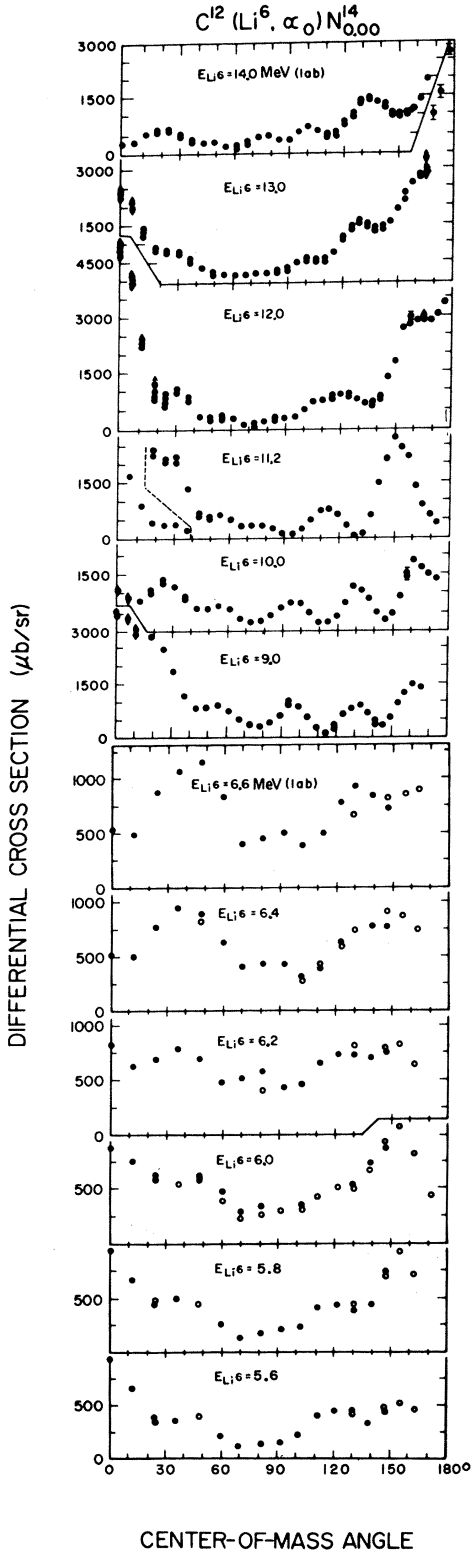

FIG. 17. Angular distributions for the α_0 group.

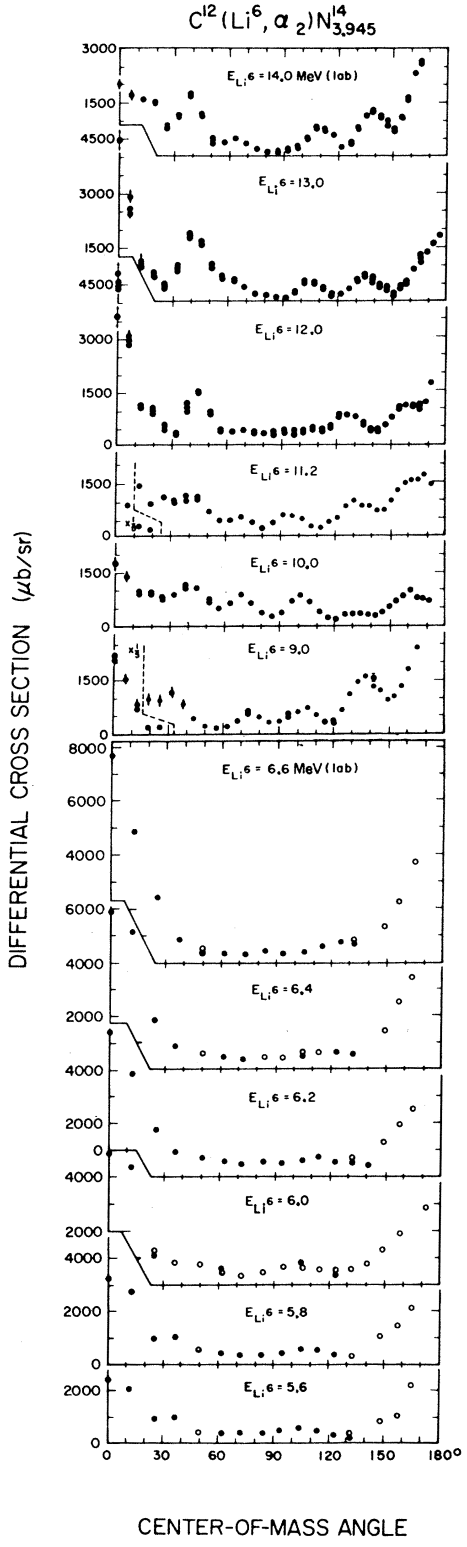

FIG. 18. Angular distributions for the α_2 group.

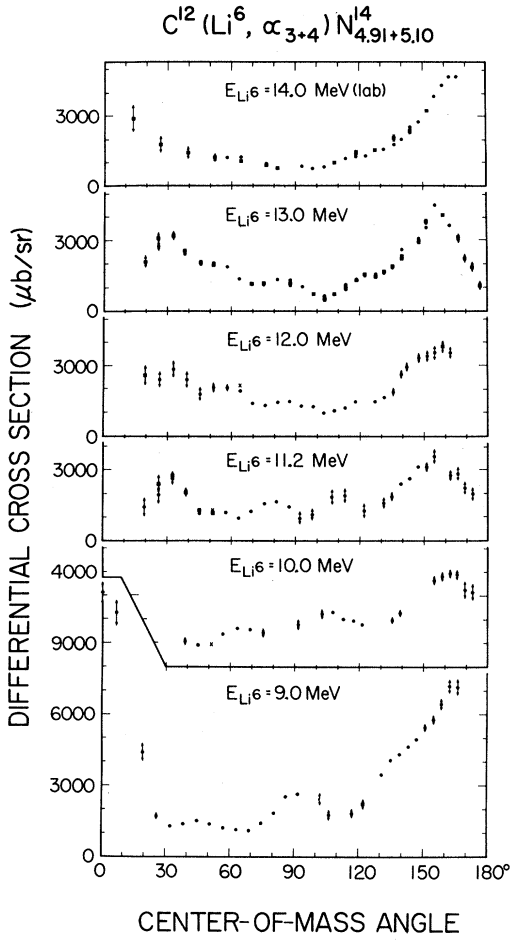

FIG. 19. Angular distributions for the $\alpha_3+\alpha_4$ groups.

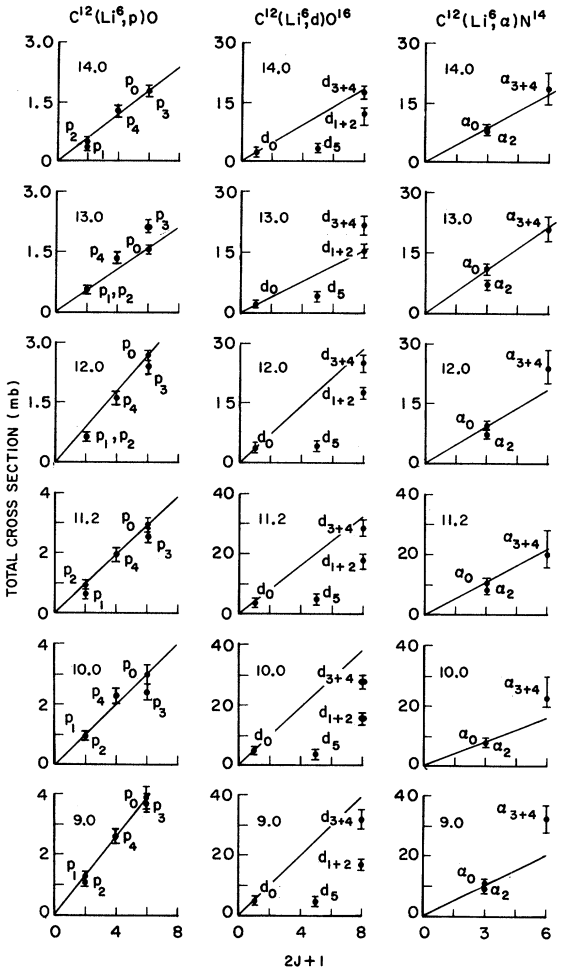

FIG. 20. Total cross section as a function of $2J+1$ for all groups.

ranging from 0 to 5.4 F. At 14.0 MeV, for $L=2$ and $R=0.0$, the calculated distributions had a minimum at 0° and a broad peak at approximately 45°. This peak moved in to 20° for $R=5.4$ F, and in all cases the differential cross section continued to decrease with increasing θ beyond this peak. The calculations with $L=0$ and $R=0.0$ had only one peak, at 0°, whereas when $R=2.75$ F the calculated distributions had, in addition to a peak at 0°, a second peak at approximately 50° of about one fourth the height of the 0° peak. These angular distributions varied little in the energy interval from 9.0 to 14.0 MeV, and displayed a shape which in no

TABLE II. Optical-model parameters.

Reaction	V (MeV)	W (MeV)	R_1 (F)	R_2 (F)	a (F)	b (F)	χ^2	$f(x)$
Li^6+C^{12}								
Set A	171.0	7.24	3.04	3.33	0.67	0.72	6.27	*sd*
Set B	136.8	7.75	3.48	3.27	0.64	0.77	6.68	*sd*
Set C	173.7	6.55	2.85	3.89	0.64	0.80	9.61	*sd*
$\alpha+N^{14}$	154.1	4.74	3.45	4.37	0.56	0.65	14.47	*sd*
$d+O^{16}$	50.0	16.00	3.80	3.80	0.70	0.70	···	*V*
p_0,p_1+O^{17}	49.2	2.9	3.21	3.21	0.62	1.6	···	*G*
p_2,p_3,p_4+O^{17}	49.2	8.6	3.21	3.21	0.54	0.4	···	*G*

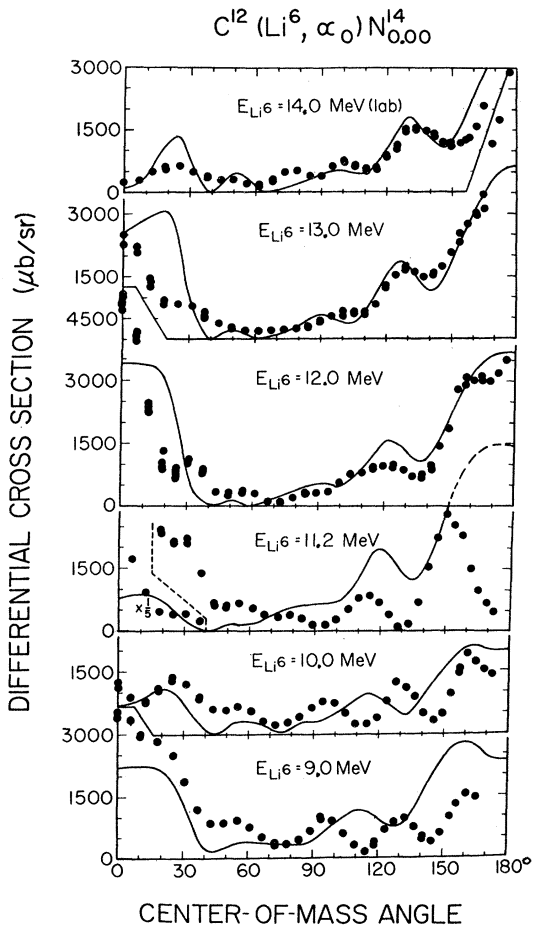

FIG. 21. Plane-wave two-mode direct-reaction fits.

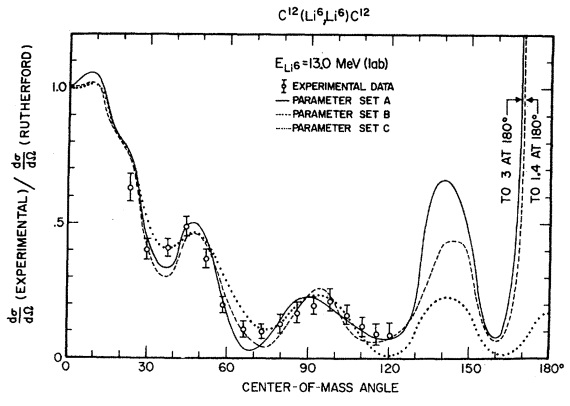

FIG. 22. Optical-model fits to Li^6+C^{12} elastic scattering data at a Li^6 bombarding energy of 13.0 MeV. See Table II for the expression for the optical-model potential used and for the values of the optical-model parameters obtained from the fits.

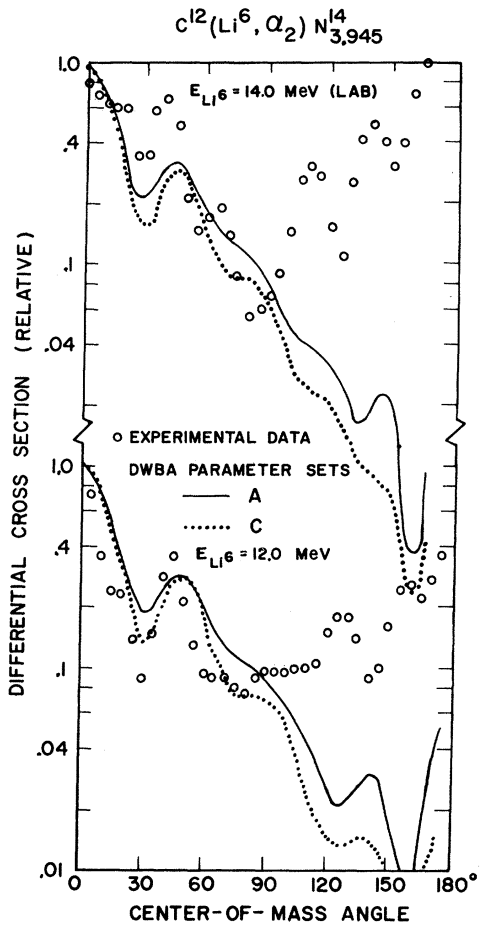

FIG. 23. A comparison of angular distributions calculated according to the DWBA model and experimental data obtained for the α_2 group.

way corresponded to the experimental angular distributions.

The second-excited-state experimental angular distributions have a peak in the region of 40° to 45°, which remains nearly fixed in the energy interval from 12.0 to 14.0 MeV. A similar peak appears in the same reaction at 20.0 MeV according to the data of Meier-Ewert, Bethge, and Pfeiffer[14] – and in the $C^{12}(He^3,p_2)N^{14}_{3.945}$ reaction according to the data of Mangelson, Harvey, and Glendenning[15] at a He^3 bombarding energy of 20.0 MeV.

DWBA ($L=0$) stripping calculations were made for the $C^{12}(Li^6,\alpha_2)N^{14}_{3.945}$ reaction at Li^6 bombarding energies of 12.0 and 14.0 MeV. The results of these calculations for optical-model-parameter Sets A and C (Table II) are shown in Fig. 23. The general character of the forward portions of the experimental angular distributions is well represented at both energies, although the calculated peaks occur at 5° larger angles in both cases. Since slight shifts in the optical-model parameters

did not help the forward-angle fits and also did not cause the backward-angle results to rise appreciably, it appears doubtful whether it will be possible to improve the fits with other optical-model parameters considering only stripping to be present.

B. Statistical Compound-Nucleus Model

A criterion established by Ericson[16] as necessary for the application of the statistical compound-nucleus (SCN) model to be valid is that the average width of an individual state should be greater than the average spacing of states in the compound system, i.e., $\Gamma_0/D \gg 1$. Using Lang's[17] level-density formula to estimate D_J and assuming $\Gamma_0 = 500$ keV (determined from an autocorrelation analysis of the experimental data discussed below and the dependence of Γ_0 upon excitation energy given by Ericson and Mayer-Kuckuk[18]), we obtain the following values of Γ_0/D_J for F^{18} at 21.0-MeV excitation for successively increasing values of J from 0 through 6: 34.4, 84.5, 92.0, 77.5, 37.0, 15.5, and 5.0. This indicates that the criterion of Ericson is satisfied for compound-nucleus levels with spins up to $J = 6$.

1. *Hauser-Feshbach Averaged Angular Distribution*

The Hauser-Feshbach (HF) expression[19] was used to calculate the averaged differential cross sections.

$$\left\langle \frac{d\sigma_{cc'}}{d\Omega}(\theta) \right\rangle = B \sum_{\substack{sls'l' \\ LJ}} (-1)^{s-s'} \overline{Z}(lJlJ; sL)\overline{Z}(l'Jl'J; s'L) \times P_L(\cos\theta) \frac{T_c(l)T_{c'}(l')}{(2J+1)e^{-J(J+1)/2\sigma^2}}, \quad (1)$$

where

$$B = \frac{D_0}{\Gamma_0} \frac{\lambda^2}{(2I+1)(2i+1)}, \quad (2)$$

I and i are the spins of the target and incoming particle, s and s' are the entrance- and exit-channel spins, l and l' are the relative angular momenta of the two particles in the entrance and exit channels, respectively, the $\overline{Z}$ coefficients are defined by Feshbach,[20] the $P_L(\cos\theta)$ are Legendre polynominals, $T_c(l)$ and $T_{c'}(l')$ are transmission coefficients for the entrance and exit channels, σ is the spin cutoff parameter, and $1/\lambda$ is the magnitude of the wave vector of the incident particle.

The entrance- and exit-channel transmission coefficients were calculated using the ABACUS-2 code[21] with the following optical-model parameters For the $Li^6 + C^{12}$ entrance channel the parameters were the same (parameter Set A of Table II) as those determined for the DWBA analysis of the $C^{12}(Li^6, \alpha)N^{14}$ reaction. Data were not available for the $p + O^{17}$ channels, and optical parameters obtained for $p + O^{16}$ elastic scattering at 15.6 and at 11.9 MeV (lab) by Duke[22] were used for the p_0 and p_1 groups and for the p_2, p_3, and p_4 groups, respectively. The spin-orbit potentials given by Duke were set equal to zero in these calculations. For the $d + O^{16}$ channel, parameters obtained by Nguyen[23] at 14.0 MeV (lab) were used. The optical parameters used for the various channels are given in Table II. The matching radius was set equal to $R_1 + 10a$ in these calculations.

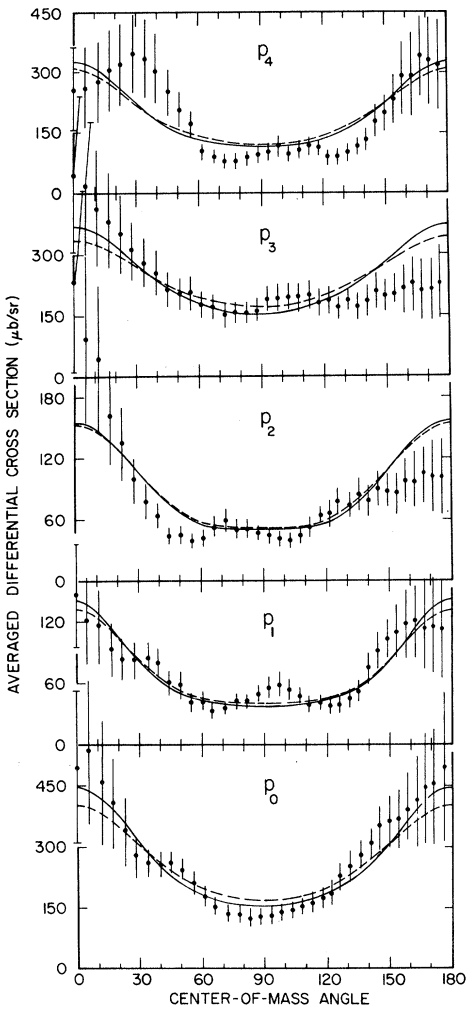

FIG. 24. Angular distributions for protons averaged over the energy interval from 9.0 to 14.0 MeV. The error bars represent FRD errors. The continuous curves represent HF averaged angular distributions calculated with a spin cutoff parameter of $\sigma = 2.16$. The broken lines represent HF averaged angular distributions obtained using $\sigma = 2.50$.

The results of these HF calculations are shown in Figs. 24 and 25. The error bars shown are the finite-range-of-data (FRD) errors due to the finite energy interval over which the differential cross sections are averaged, and are given by[24]

$$\frac{\Delta\langle d\sigma/d\Omega\rangle}{\langle d\sigma/d\Omega\rangle}=\left[\frac{\pi C_{\exp}(\epsilon=0)}{n}\right]^{1/2}.$$

Here $\Gamma_0 n$ is the energy interval over which the angular distributions are averaged and $C_{\exp}(\epsilon=0)$ is taken from the autocorrelation function $C_{\exp}(\epsilon)$ discussed below.

The HF averaged angular distributions plotted as continuous lines in Figs. 24 and 25 were calculated using a spin cutoff parameter σ of 2.16, whereas those plotted with broken lines were calculated with $\sigma=2.5$. The value $\sigma=2.16$ was calculated for the compound nucleus F^{18} at 21.0-MeV excitation energy using[17] $\sigma^2=cT$, where $c\hbar^2$ is the rigid-body moment of inertia for the Fermi-Thomas model of the compound nucleus, and T is the thermodynamic temperature at an energy of excitation at the midpoint of the interval spanned. Calculations using $\sigma=2.5$ are also presented here, because they gave reasonable fits for most particle groups, and the normalization constants B obtained for the various groups were more nearly the same. The values of B obtained for $\sigma=2.16$ and 2.5 are shown in Table III.

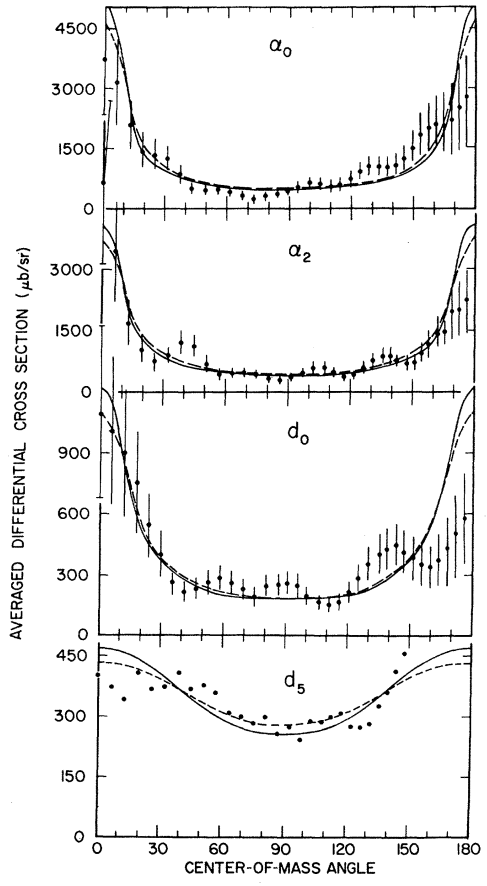

FIG. 25. Averaged angular distributions for α particles and deuterons. See caption of Fig. 24.

The variation of the relative sizes of the normalization constants as a function of particle type is similar to that of the ratios of averaged experimental to HF averaged differential cross sections obtained at 0° by Dzubay[25] for p_0, p_1, p_2, p_3, d_0, and α_0 groups, namely, 0.43, 0.33, 1.01, 0.88, 0.46, and 0.60, respectively. Though the shapes of the predicted HF averaged angular distributions are quite insensitive to the optical-model parameters used, the values of the normalization constant B are very sensitive to the optical parameters used. This sensitivity is illustrated by the fact that the values of B for the p_2, p_3, and p_4 groups become 3.02, 2.43, and 3.38×10^{-30} cm^2, respectively, when the optical-model parameter set for the p_0 and p_1 groups is used with $\sigma=2.50$. If a representative normalization constant $B=2.0\times10^{-30}$ cm^2 is substituted into Eq. (2), one obtains $\Gamma_0/D_0=28.3$, which is certainly within the order-of-magnitude agreement one might expect with the value of 34.5 one obtains from Lang's[17] level-density formula assuming $\Gamma_0=500$ keV.

It is interesting to compare the results of the present HF calculations with the experimental total cross sections $\sigma_{\exp}$, interpreted in terms of the $(2J+1)$ rule[26] shown in Fig. 21. The simplest form of the rule states that the total cross section for a given reaction should be proportional to $2J+1$, where J is the spin of the residual nucleus, and is often used as a test of the SCN model. However, the rule, so stated, does not allow for variation in exit-channel transmission coefficients for different particle groups. Only if this variation is negligible should σ_{SCN} be equal to a constant times $(2J+1)$.

If the SCN model described the reaction process for all channels, the normalization constant B should be the same for all groups. In this analysis, for $\sigma=2.5$, the value of B was approximately 2 for the p_0 and p_1 groups, but 4.5, 4, and 5.5 for p_2, p_3, and p_4, respectively. In other words, if the reactions involving the p_0 and p_1 groups are described by the HF formalism of the SCN model, the exper-

TABLE III. Values of normalization constant B (10^{-30} cm^2).

σ	p_0	p_1	p_2	p_3	p_4	d_0	d_5	α_0	α_2
2.16	0.788	1.24	3.29	1.91	3.42	0.71	1.33	0.141	0.494
2.50	1.89	1.91	4.56	3.81	5.59	2.11	2.50	2.24	3.00

imental cross sections for the p_0, p_3, and p_4 groups are factors of 2 to 3 times as large as the prediction of the SCN model. But the $(2J+1)$ plots in Fig. 21 show σ_{exp} for all proton groups closely proportional to $(2J+1)$.

The deuteron groups in Fig. 21 have σ_{exp} which are more consistent with what one would expect assuming a $(2J+1)$ rule resulting from the SCN model, in that the higher-excited-state groups have σ_{exp} which fall below the $(2J+1)$ line. It is interesting that the d_5 group has an experimental cross section approximately 5 times smaller than that predicted by $(2J+1)$ proportionality, but approximately equal to that predicted by the SCN model on the basis of the HF formalism. In the case of the α-particle σ_{exp}'s compared with the $(2J+1)$ rule, it is not clear how the σ_{3+4} group can generally have a σ_{exp} which lies near or above the line through the α_0 and α_2 cross sections if the σ_{exp}'s are described by the SCN model.

These considerations illustrate that one must be very careful in interpreting the results of the application of the simple form of the $(2J+1)$ rule, particularly when near the Coulomb barrier where transmission coefficients are varying rapidly as a function of energy.

The agreement between the general shapes of the calculated HF averaged angular distributions and the averaged experimental angular distributions is satisfactory for some groups but unsatisfactory for others, as can be noted from Figs. 24 and 25. The best agreement between theoretical and experimental data occurs for the p_0 and p_1 groups with somewhat less agreement observed for the p_4, α_0, and α_2 groups. An unsatisfactory agreement, characterized by a tendency for the experimental data points to lie above the HF curves at forward angles and below the curves at backward angles, is noted for the p_2, p_3, and d_0 groups.

It is possible that some of this disagreement is due to direct-reaction contributions at forward angles. Direct-reaction contributions might also explain the fact that the value of B for groups that have this forward-peaking effect is generally larger than it is for groups which do not have the peaking.

2. *Autocorrelation Functions*

Autocorrelation functions were evaluated, as prescribed by Ericson[16], for each of the yield curves shown in Figs. 5 and 6, corresponding to resolved groups. To correct for the energy dependence of the cross section due to the Coulomb barrier, a useful technique which has been applied by Dallimore and Allardyce[27] was used. In this method the differential cross-section values are divided by a relative cross section, which represents the expected smooth energy dependence of the yield-curve points, before calculating the autocorrelation function. In the energy interval from 4.0 to 8.6 MeV, the HF averaged differential cross sections of Dzubay[25] were used for the smoothly varying cross section. Above 8.0 MeV, the energy dependence of the differential cross sections were estimated from the experimental total cross sections at 9.0, 10.0, 11.2, 12.0, 13.0, and 14.0 MeV.

The values of $C_{exp}(\epsilon = 0)$ and Γ_0 obtained from the autocorrelation-function calculations are shown in Table III. All values were taken from autocorrelation functions determined using the HF correction method except those for $\alpha_0(0°)$ and $\alpha_2(40°)$, which were determined from autocorrelation functions obtained by the base-line-shift method[27,28] and obtained without corrections, respectively. The base base-line-shift method[28] was applied because the α_0 autocorrelation function did not have the Lorentzian shape given by $(\Gamma_0)^2/(\Gamma_0^2 + \epsilon^2)$ but appeared to be too large at $\epsilon = 0$ and passed far below 0 in the region of $\epsilon = 6.0$ MeV. Also two or three oscillations in the autocorrelation function for this group provided a basis for selecting a base line. No correction was made in the autocorrelation function for α_2 obtained from the raw data in the energy interval from 5.0 to 14.0 MeV because the experimental cross section for this group was observed to fluctuate about a nearly constant value. All Γ_0 have been corrected for FRD effects using the method of Dallimore and Hall.[24]

Theoretical values of $C(\epsilon = 0)$, for each of the reactions studied, were calculated at $\theta_{lab} = 0°$ and 40° using an expression given by Dallimore and Hall,[24] which includes a correction for FRD effects as well as an expression for the FRD error:

$$C_{theor}(\epsilon = 0) \simeq \frac{1}{N} - \frac{(N+1)}{nN^2} \pm \frac{(N+1)^{1/2}}{nN^3} , \qquad (3)$$

where $n\Gamma_0$ is the energy interval represented and N is the spin damping factor.

In these calculations it was assumed that N takes on its maximum value at $\theta_{lab} = 40°$, a reasonable assumption since the coherence angle δ for $Li^6 + C^{12}$ reactions over the energy interval studied is much less than 40°, as shown below. The calculated theoretical values of $C(\epsilon = 0)$ are given in Table IV.

Even though we now have yield-curve measurements for Li^6 bombarding energies from 4.0 to 14.0 MeV, the FRD errors are still very large and preclude much in the way of meaningful comment on the results. When dealing with a situation where Γ_0 is of the order 0.500 MeV, a 10-MeV energy range does not give a large sample size. One also has to work with the problem that Γ_0 changes

TABLE IV. Results of autocorrelation analysis. All results were obtained using HF-corrected autocorrelation functions unless otherwise noted.

Particle group	$\theta_{lab}=0°$ C_{theory} ($\epsilon=0$)	$\theta_{lab}=0°$ C_{exp} ($\epsilon=0$)	$\theta_{lab}=0°$ Γ_0 (keV)	$\theta_{lab}=40°$ C_{theory} ($\epsilon=0$)	$\theta_{lab}=40°$ C_{exp} ($\epsilon=0$)	$\theta_{lab}=40°$ Γ_0 (keV)
p_0	0.36 ± 0.27	0.71	960	0.05 ± 0.03	0.04	315
p_1	0.36 ± 0.27	0.58	560	0.13 ± 0.08	0.19	396
p_2	0.36 ± 0.27	0.28	780	0.13 ± 0.08	0.11	200
p_3	0.36 ± 0.27	0.53	780	0.05 ± 0.03	0.11	470
d_0	0.36 ± 0.27	0.42	470	0.16 ± 0.09	0.18	396
α_0	0.36 ± 0.27	0.64[a]	475[a]	0.16 ± 0.09	0.19	515
α_2	0.25 ± 0.35	0.15	390	0.16 ± 0.09	0.16[b]	436[b]

[a] Obtained from a base-line corrected autocorrelation function.
[b] Obtained from an uncorrected autocorrelation function.

markedly over even a 10-MeV energy range.

3. *Angular Cross-Correlation Function*

To further test the validity of the SCN model as applied to these data, angular cross-correlation functions[29] for the experimental data were determined for several of the particle groups. The coherance angles obtained from these angular cross-correlation functions for the various particle groups are as follows: p_0, 20°; p_1, 18°; p_2, 20°; p_3, 15°; p_4, 19°; d_0, 16°; α_1, 16°; and α_2, 14°.

Brink, Stephen, and Tanner (BST)[29] have ob- the following expression for the coherance angle δ on the basis of a surface-emission model of SCN reactions:

$$\delta \simeq \text{max of } (1/kR,\ 1/k'R',\ \text{or } 1/J_M). \qquad (4)$$

The quantities k and k' are the center-of-mass wave numbers of the entrance- and exit-channel particles, respectively, R and R' are the radii of the target and residual nuclei, and J_M is the largest spin of the compound-nuclear states having sufficient density to give a significant contribution to the cross section.

In this experiment, at a Li^6 bombarding energy at the midpoint (11.5 MeV) of our energy interval, if we assume the target and residual nuclei to have radii given by $1.4\times A^{1/3}$, then the coherence angle δ, limited by $1/kR$ of the exit channel for protons and the entrance channel for α particles, has a value of 18.5, 19.0, 20.8, 21.5, 22.1, and 13.8° for the p_0, p_1, p_2, p_3, p_4, and d_0 groups, respectively, and 12.8° for both α-particle groups.

The fact that the d_0 and α-particle coherence angles as measured are somewhat larger than the values of 13.8° and 12.8° predicted on the basis of $1/k'R'$ and $1/kR$ may indicate that the d_0 and α-particle coherence angles are limited not by $1/kR$ but by $1/J_M$. The value of J_M can be estimated from the density of states calculated above using Lang's level-density formula. States with spins smaller or equal to $J_M=4$ include 95% of the states. Relation (4) with $J_M=4$ gives $\delta\simeq 14.4°$. The agreement between the measured and the predicted values of δ is not good (the p_3 group in particular has a deviation of 6.5°). However, the arguments of BST[29] are to a great extent qualitative, and for this reason relation (4) is expected to be in only qualitative agreement with experimental results.

VI. CONCLUSION

It had been hoped in designing this experiment, that by obtaining yield curves and angular distributions (over almost 180°) over a wide energy region above the Coulomb barrier, and by using a fairly simple target, we could come to a better understanding of Li^6 reactions – perhaps by comparison with existing reaction models. Our conclusions, however, are not particularly neat. The evidence presented indicates that neither the direct-reaction nor the statistical compound-nucleus model alone is adequate to describe the existing data. And, in fact, it looks as if it would be difficult for a combination of the two models to describe the data adequately. Some more sophisticated model appears to be required to describe the Li^6+C^{12} reaction data obtained. The change may need to be in the models of the nuclei involved – it is not new for reactions involving Li or C^{12} to exhibit features which are difficult to explain.

ACKNOWLEDGMENTS

We wish to thank Professor Richard R. Carlson for his suggestions and interest during the statistical-model analysis.

*Research supported in part by the National Science Foundation.

†Present address: Air Force Weapons Laboratory, Kirtland Air Force Base, New Mexico 87117.

[1]T. Lauritsen and F. Ajzenberg-Selove, *Nuclear Data Sheets*, compiled by K. Way *et al.* (Printing and Publishing Office, National Academy of Sciences – National Research Council, Washington, D.C., 1962), NRC 61-5-6.

[2]T. K. Alexander, C. Broude, A. E. Litherland, Nucl. Phys. 53, 593 (1964).

[3]D. J. Johnson, M. S. Thesis, University of Iowa Report No. 67-45, 1967 (unpublished).

[4]D. W. Heikkinen, Phys. Rev. 141, 1007 (1966).

[5]C. F. Williamson, J. Boujot, and J. Picard, Centre D'Etudes Nucleaires de Saclay Report No. CEA-R 3042, 1966 (unpublished).

[6]T. Fulton and G. E. Owen, Phys. Rev. 108, 789 (1957).

[7]S. Edward, Tandem Van de Graaff Accelerator Laboratory, Florida State University, Tallahassee, Florida, Notes by L. L. Warsh, October, 1961 (unpublished).

[8]M. A. Waggoner and A. A. Jaffe, Nucl. Phys. 69, 305 (1965); F. D. Snyder and M. A. Waggoner, University of Iowa Report No. 69-20, 1969 (unpublished); Phys. Rev. 186, 999 (1969).

[9]D. R. Inglis, Rev. Mod. Phys. 25, 390 (1953); Phys. Rev. 126, 1789 (1962).

[10]W. M. Visscher and R. A. Ferrell, Phys. Rev. 107, 781 (1957).

[11]W. R. Gibbs, V. A. Madsen, J. A. Miller, W. Tobocman, E. C. Cox, and L. Mowry, National Aeronautics and Space Administration Report No. NASA TND-2170 (unpublished).

[12]W. R. Smith, University of Southern California Report No. USC-136-119 (unpublished).

[13]W. D. Ploughe, Phys. Rev. 122, 1232 (1961).

[14]K. Meier-Ewert, K. Bethge, and K. O. Pfeiffer, Nucl. Phys. A110, 142 (1968).

[15]N. F. Mangelson, Bernard G. Harvey, and N. K. Glendenning, Nucl. Phys. A117, 161 (1968).

[16]T. Ericson, Ann. Phys. (N.Y.) 23, 390 (1963); Advan. Phys. 9, 425 (1960).

[17]D. W. Lang, Nucl. Phys. 26, 434 (1961).

[18]T. Ericson and T. Mayer-Kuckuk, Ann. Rev. Nucl. Sci. 16, 183 (1966).

[19]W. Hauser and H. Feshbach, Phys. Rev. 87, 366 (1952); A. Richter, A. Bamberger, P. von Bretano, T. Mayer-Kuckuk, and W. von Witsch, Z. Naturforsch 21a, 1002 (1966).

[20]H. Feshbach, *Nuclear Spectroscopy*, edited by F. Ajzenberg-Selove (Academic Press Inc., New York, 1960), Part B.

[21]E. H. Auerbach, Brookhaven National Laboratory Report No. BNL-6562.

[22]C. B. Duke, Phys. Rev. 129, 681 (1963).

[23]D. Nguyen, J. Phys. Soc. Japan 21, 2462 (1966).

[24]D. J. Dallimore and I. Hall, Nucl. Phys. 88, 193 (1966).

[25]T. G. Dzubay, Phys. Rev. 158, 977 (1967).

[26]N. Macdonald, Nucl. Phys. 33, 110 (1962).

[27]P. J. Dallimore and B. W. Allardyce, Nucl. Phys. A108, 150 (1968).

[28]L. W. Put, J. D. A. Roeders, and V. van der Woude, Nucl. Phys. A112, 561 (1968).

[29]D. M. Brink, R. O. Stephen, and N. W. Tanner, Nucl. Phys. 54, 577 (1964).

PHYSICAL REVIEW C VOLUME 2, NUMBER 1 JULY 1970

Relationship Between the Triton Energy and the Neutron-Deuteron Doublet Scattering Length*

T. Brady,† E. Harms,‡ L. Laroze,§ and J. S. Levinger

Department of Physics and Astronomy, Rensselaer Polytechnic Institute, Troy, New York 12181

(Received 30 March 1970)

Phillips found a linear relation between the triton energy E_t and the doublet n-d scattering length ^2a for a variety of separable tensor potentials. We have treated many more separable potentials, and also the Tabakin and Mongan rank-two separable potentials. The linear relation holds well for two-body potentials that fit the energies of the two-body triplet bound and singlet antibound states.

I. INTRODUCTION

In this paper we present a number of calculations of the triton energy (E_t) and the doublet n-d scattering length (^2a) supporting the linear relation between these two quantities found by Phillips.[1] Phillips used Yamaguchi[2] singlet and triplet two-body potentials, and obtained different linearly related values of E_t and ^2a when he varied either the singlet effective range or the deuteron percent D state (P_D). He kept constant both the deuteron energy and the energy of the singlet antibound state. Karchenko, Petrov, and Storozhenko[3] varied the exponent n in modified singlet and central triplet form factors: $g(p) = (p^2+\beta^2)^{-n}$. The value $n=1$ gives the Yamaguchi shape used by Phillips; the values $n=2$ and 3 give additional points on the Phillips line, shown in Fig. 1. We also show calculated values using a central spin-dependent separable potential.[3]